Examination of a Methane/Diesel RCCI Engine using Pele

Preprint

Nicholas T. Wimer,[1] Lucas Esclapez,[1] Marc Henry de Frahan,[1] Mohammad Rahimi,[1] Malik Hassanaly,[1] Bruce Perry,[1] Jon Rood,[1] Shashank Yellapantula,[1] Hariswaran Sitaraman,[1] Michael Martin,[1] Olga Doronina,[1] Sreejith Nadakkal Appukuttan,[1] Martin Reith,[2] and Marc Day[1]

1 National Renewable Energy Laboratory
2 Sandia National Laboratory

Presented at the 13th U.S. National Combustion Meeting
College Station, Texas
March 19–22, 2023

NREL is a national laboratory of the U.S. Department of Energy
Office of Energy Efficiency & Renewable Energy
Operated by the Alliance for Sustainable Energy, LLC

This report is available at no cost from the National Renewable Energy Laboratory (NREL) at www.nrel.gov/publications.

Contract No. DE-AC36-08GO28308

Conference Paper
NREL/CP-2C00-84700
May 2023

Examination of a Methane/Diesel RCCI Engine using Pele

Preprint

Nicholas T. Wimer,[1] Lucas Esclapez,[1] Marc Henry de Frahan,[1] Mohammad Rahimi,[1] Malik Hassanaly,[1] Bruce Perry,[1] Jon Rood,[1] Shashank Yellapantula,[1] Hariswaran Sitaraman,[1] Michael Martin,[1] Olga Doronina,[1] Sreejith Nadakkal Appukuttan,[1] Martin Reith,[2] and Marc Day[1]

1 National Renewable Energy Laboratory
2 Sandia National Laboratory

Suggested Citation
Wimer, Nicholas T., Lucas Esclapez, Marc Henry de Frahan, Mohammad Rahimi, Malik Hassanaly, Bruce Perry, Jon Rood, Shashank Yellapantula, Hariswaran Sitaraman, Michael Martin, Olga Doronina, Sreejith Nadakkal Appukuttan, Martin Reith, and Marc Day. 2023. *Examination of a Methane/Diesel RCCI Engine using Pele: Preprint*. Golden, CO: National Renewable Energy Laboratory. NREL/CP-2C00-84700. https://www.nrel.gov/docs/fy23osti/84700.pdf.

NREL is a national laboratory of the U.S. Department of Energy
Office of Energy Efficiency & Renewable Energy
Operated by the Alliance for Sustainable Energy, LLC

This report is available at no cost from the National Renewable Energy Laboratory (NREL) at www.nrel.gov/publications.

Contract No. DE-AC36-08GO28308

Conference Paper
NREL/CP-2C00-84700
May 2023

National Renewable Energy Laboratory
15013 Denver West Parkway
Golden, CO 80401
303-275-3000 • www.nrel.gov

NOTICE

This work was authored in part by the National Renewable Energy Laboratory, operated by Alliance for Sustainable Energy, LLC, for the U.S. Department of Energy (DOE) under Contract No. DE-AC36-08GO28308. This research was supported by the Exascale Computing Project (ECP), Project Number: 17-SC-20-SC, a collaborative effort of two DOE organizations, the Office of Science and the National Nuclear Security Administration. The views expressed herein do not necessarily represent the views of the DOE or the U.S. Government. The U.S. Government retains and the publisher, by accepting the article for publication, acknowledges that the U.S. Government retains a nonexclusive, paid-up, irrevocable, worldwide license to publish or reproduce the published form of this work, or allow others to do so, for U.S. Government purposes.

Examination of a Methane/Diesel RCCI Engine using Pele

Nicholas T. Wimer[1,*], *Lucas Esclapez*[1], *Marc Henry de Frahan*[1], *Mohammad Rahimi*[1], *Malik Hassanaly*[1], *Bruce Perry*[1], *Jon Rood*[1], *Shashank Yellapantula*[1], *Hariswaran Sitaraman*[1], *Michael Martin*[1], *Olga Doronina*[1], *Sreejith Nadakkal Appukuttan*[1], *Martin Reith*[2], *and Marc Day*[1]

[1]*National Renewable Energy Laboratory, 15013 Denver W Pkwy, Golden, CO 80401, US*

[2]*Sandia National Laboratory, 1515 Eubank Blvd SE1515 Eubank Blvd SE, Albuquerque, NM 87123, US*

[*]*Corresponding author:* nicholas.wimer@nrel.gov

Abstract: Multi-fuel, advanced injection strategies have become increasingly promising as a strategy to mitigate the emissions generated from internal combustion engines. By carefully controlling the combustion phasing in-cylinder, these new multi-pulse, multi-fuel injection strategies are able to burn in the low-temperature combustion regime where both NO_x and soot are not readily produced, reducing the need for extensive exhaust gas recirculation systems. In this study, we examine a reactivity-controlled compression ignition (RCCI) strategy that uses an early pre-filled methane-air mixture with low turbulence background as the low-reactivity fuel and a direct injection of four discrete dodecane jets as a surrogate for the high-reactivity diesel fuel. We use the Pele software suite, a highly optimized, exascale-ready, adaptive mesh refinement codebase to perform high-resolution numerical simulations of a scaled down, single cylinder from the RCCI engine. Here, we resolve the ignition kernels down to micrometer scales and present several statistical quantities evaluating the development of the flow and detailing the onset of ignition and subsequent flame development. Particular attention is paid to the conditions surrounding the onset of the first ignition kernels and discussing what led to the development of those conditions.

Keywords: reactivity-controlled compression ignition engine, exascale, pele, combustion, simulation

1. Introduction

Compression-ignition (CI) engines operate by introducing fuel to the high-temperature, high-pressure environment created by piston compression of in-cylinder gases. CI engines typically directly inject a high-reactivity fuel (HRF) into the cylinder near the top of the piston stroke at top-dead-center (TDC), where the temperature and pressure are at their pre-ignition peaks. The HRF fuel stream mixes with the surrounding oxidizer stream and auto-ignites, resulting in a sharp increase in pressure, driving the piston downwards, rotating a crank shaft, thereby extracting work from the engine. While effective, this conventional diesel combustion (CDC) strategy predominantly burns fuel in a high-equivalence ratio, high-temperature environment that is known to produce a great deal of soot and NO_x [1]. In an effort to reduce the emissions generated by CI engines while retaining the benefits of CDC, many advance compression ignition (ACI) strategies have

emerged that aim to burn fuel in the low-temperature combustion (LTC) regime, where both NO_x and soot are not readily produced.

One of the more prominent ACI strategies is reactivity-controlled compression ignition (RCCI) [2], which operates by directly injecting a HRF though one or more pulses into a homogeneous mixture of an oxidizer and a low-reactivity fuel (LRF). Through careful control of the injection timing and dual-fuel properties, RCCI enables burning the combined fuels at leaner conditions and lower temperatures than CDC strategies. There have been a wide range of both experimental and computational studies examining various aspects of RCCI design, optimization, and performance throughout the literature. Experimental studies has examined performed parametric sweeps over the range of LRF/HRF to determine promising combinations of fuel types under different engine operating parameters [3]. Computational studies have been focused on gaining more insight in the mechanism of fuel reactivity stratification on combustion phasing through a series of largely 2D direct numerical simulation (DNS) [4–6] and more recently 3D large-eddy simulation (LES) [7].

There are a number of computational challenges associated with performing a three-dimensional DNS of a realistic RCCI engine setup. The DNS would consist of billions of computational cells to resolve down to the sub-micrometer scale, requiring the computational fluid dynamics (CFD) software to be highly-scalable. Large amount of computing resources would be required to evolve these billions of cells for at least up to 1 ms to allow for appropriate fuel mixing and ignition delay. Additionally, the incorporation of complex geometry and detailed chemistry would be required for an accurate assessment of the combustion mechanism in the context of real-world cylinder design.

In this paper, we present our development of two different exascale-ready, CFD codes capable of achieving highly resolved numerical simulations of an RCCI engine under realistic conditions approaching DNS scales. First we detail the numerical methodology of the fully-compressible (PeleC) and low-Mach (PeleLMeX) adaptive mesh refinement (AMR) CFD software codes and the development required for realistic RCCI engine simulation. We then show the RCCI setup and operating parameters for the simulations. Finally, we show the results of the simulations using both tools, discuss the differences between the codes and implications of the onset of the first ignition kernels.

2. Methods

In this section we present the numerical frameworks for both the fully-compressible and low-Mach CFD combustion codes. We discuss the similarities and key differences between the assumptions made in both codes and provide a brief background on their development paths. We then show the computational setup of the RCCI engine simulation: geometry, initial conditions, boundary conditions, fuel properties, and chemical reaction mechanism details.

2.1 Numerical frameworks

The simulations presented in this work were conducted with the Pele suite of codes [8], more particularly the multi-species Navier-Stokes compressible solver PeleC [9] and its low-Mach number counterpart PeleLMeX [10]. Both solvers utilize a finite volume approach with block-structured AMR and are built upon the AMReX library [11] designed to leverage the computational power of emerging ExaScale platforms, such as the new Frontier HPC machine based out of Oak Ridge National Laboratory (ORNL). Additionally, the solvers share the implementation of the transport and

equation of state evaluation as well as the chemistry description (including thermodynamics and chemical kinetics) through PelePhysics [12]. While both codes share many of the same routines and physical implementations, there are differences, specifically with respect to the implementation of the low-Mach assumption and related algorithms. The algorithmic details and differences of both solvers are described below.

2.1.1 PeleC

PeleC is the fully-compressible solver built on the Pele suite of codes that features AMR, various combustion models, embedded boundaries (EBs) for complex geometries, and non-ideal equations of state. PeleC solves the conservative equations for mass, species mass fractions, momentum, and energy with a finite rate evaluation of chemistry in the compressible regime.

PeleC time-advancement is based on a 2^{nd} method-of-line scheme, where advection and diffusion terms are treated explicitly using a 2^{nd} characteristic-based spatial scheme and 2^{nd} centered differences scheme, respectively. Chemistry is integrated implicitly with CVODE [13] relying on a Jacobian free approach to solve the chemical linear system. Note that the use of this particular advection scheme in place of the less dissipative Godunov scheme is dictated by the presence of EBs.

For additional details about PeleC, please refer to: [9].

2.1.2 PeleLMeX

In contrast with PeleC, PeleLMeX solves the multispecies Navier-Stokes equations in their low Mach number limit, where the acoustic waves are mathematically removed from the equation of motion because the fluid velocity is small compared to speed of sound and compressibility effects are unimportant to the evolution of the system. The time step CFL constraint is then based on an advective velocity.

The time advancement algorithm is based on a fractional step approach extended to reactive flows [14] where the velocity divergence constraint arising from the low-Mach approximation is enforced iteratively within the spectral deferred correction (SDC) advance of the thermodynamic variables. The later is employed to ensure a tight coupling of the fast reaction and diffusion processes with the slower advection. The advection terms are treated explicitly with a 2^{nd} order Godunov scheme modified for EBs, while diffusion terms are treated semi-implicitly with a Crank-Nicholson scheme and the stiff chemistry is treated implicitly with CVODE [13]. Compared to PeleC, the large time step size requires the use of the GPU-based batched linear algebra direct solver MAGMA [15] to fully leverage the benefits of CVODE internal time-stepping scheme. Finally, PeleLMeX uses a non-subcycling algorithm to advance the AMR hierarchy, where all levels are advanced simultaneously using the same time step size, often prescribed by the finest AMR level CFL constraint. For additional details about PeleLM/PeleLMeX, please refer to: [10].

2.1.3 PelePhysics

PelePhysics is the suite of codes coupled with both PeleC and PeleLMeX that provides routines to compute thermal properties, transport properties, and chemical reaction integration for detail chemical mechanisms. PelePhysics provides routines for finite-rate chemistry integration as well

Figure 1: Visualization of the piston-bowl geometry used in the Pele simulations. EBs are used to represent the piston-bowl surface. Fuel is injected at four discrete points at the top of the domain as indicated by the blue arrows.

as a Python-based preprocessor (CEPTR) for generating C++ mechanism code for efficient evaluation of Quasi-Steady State Approximation (QSSA) chemical reaction mechanisms. These routines make direct substitutions of the QSSA to eliminate implicit evaluation, thereby making the chemical integration more accurate and less sensitive to numerical time step size [12]. Although non-QSSA mechanisms are also supported, in this work we will exclusively use a QSSA mechanism as the numerical integration was shown to be faster than the standard skeletal mechanism. For additional details about PelePhysics and CEPTR, please refer to: [9, 12].

2.2 Computational setup

The piston-bowl/cylinder geometry is based off of a scaled down, single cylinder of a CI engine. The computational domain consists of the small clearance volume remaining at the end of the piston stroke as the piston reaches TDC. The base grid is a rectangular $2.8 \times 2.8 \times 0.7$ cm domain discretized using a $512 \times 512 \times 128$ Cartesian grid. EBs are used to intersect the grid and represent a 1.2 cm radius cylinder with a profiled piston head (Figure 1). The cylinder is initially filled with a homogeneous methane/air mixture at equivalence ratio of $\phi = 0.5$, which would physically correspond to a LRF introduced into the cylinder by means of a port fuel injection. The initial temperature and pressure of the domain is set to 900 K at 60 atm., which is determined from the adiabatic compression of the same initial cylinder gas from a CI engine with a compression ratio of 16.2. The initial velocity field is initialized at a low-level turbulent intensity representative of the swirl from the piston-bowl geometry.

Dodecane fuel is direct injected into the cylinder from the top of the domain by means of four discrete jets with diameter of 170 μm at an angle of 45 $^\circ$ degrees from the vertical direction. The start of the fuel injection coincides with the start of the simulation and proceeds for 0.5 ms at which point the mass flow rate injector is quickly ramped down by a hyperbolic tangent function. Both simulations are then evolved in time until 1.0 ms is reached. Each of the simulations resolves the jet structure through AMR selectively refined based on temperature gradient and vorticity magnitude. The simulations use up to four grid levels to resolve the physical scale down to approximately 6.8 μm using in excess of 2 billion computational cells.

Table 1: Operating conditions for the RCCI engine simulations in PeleC and PeleLMeX

Background mixture					
Pressure [atm]	Temperature [K]	ϕ [-]	Composition [-]		
60	900	0.5	CH_4:0.02059 O_2:0.16431 N_2:0.81510		
Fuel jets					
Temperature [K]	Mean velocity [m/s]	N_j [-]	r_{inj} [μm]	Angle [$^\circ$]	Z [-]
450	28	4	85	45	0.45

In these simulations, we do not model a moving piston, but instead apply the assumption that the chemical and advection timescales are much faster than the timescale associated with the piston motion. In doing so, we do not account for the slight decrease in pressure associated with the piston's downward motion after the onset of ignition.

3. Results

Here, we present the results from both of the high-resolution numerical simulation of the RCCI engine cylinder. We show and discuss several physical quantities of interest through quantitative and qualitative figures to examine the onset of LTC.

3.1 Qualitative comparisons

The primary difference between the two computational solvers is the handling of the low-Mach assumption which manifests itself in the advection and diffusion schemes. These differences will result in different jet development and mixing of the fuel streams with the ambient oxidizer/LRF background.

Figure 2 shows the development of both PeleC and PeleLMeX at various timesteps throughout the simulation by means of two-dimensional slices of the fuel mass fraction. The structure of the jets is qualitatively similar at the three instances in time, however, close examination will reveal that there is more coherent fuel structure noted in the PeleC results. The PeleLMeX results, on the other hand, show slightly more enhanced turbulent mixing particularly along the shear interface between the fuel jets and the ambient fluid. Additionally, at the later time of 0.9 ms, the low-Mach jet has spread to a greater width and appears to be more disperse than its fully-compressible counterpart.

Figure 3 shows the same time snapshots as in Figure 2, but now visualizing the temperature field as well as contours of two species that have been shown to be indicators to LTC [7]. These figures show similar structural developments, but with PeleLMeX showing much earlier start to the development of the long-chain hydrocarbon (Y(OC12H23OOH)) along the boundary of the jet. The development of these indicators of LTC is associated with the enhanced mixing between the fuel and surrounding pre-heated oxidizer/LRF mixture as noted in Figure 2. Figure 3 shows that at later time snapshots, PeleLMeX is further along in the combustion process due to the earlier onset of combustion than in the fully-compressible simulation, as indicated by the higher peak temperature and larger regions of high temperature.

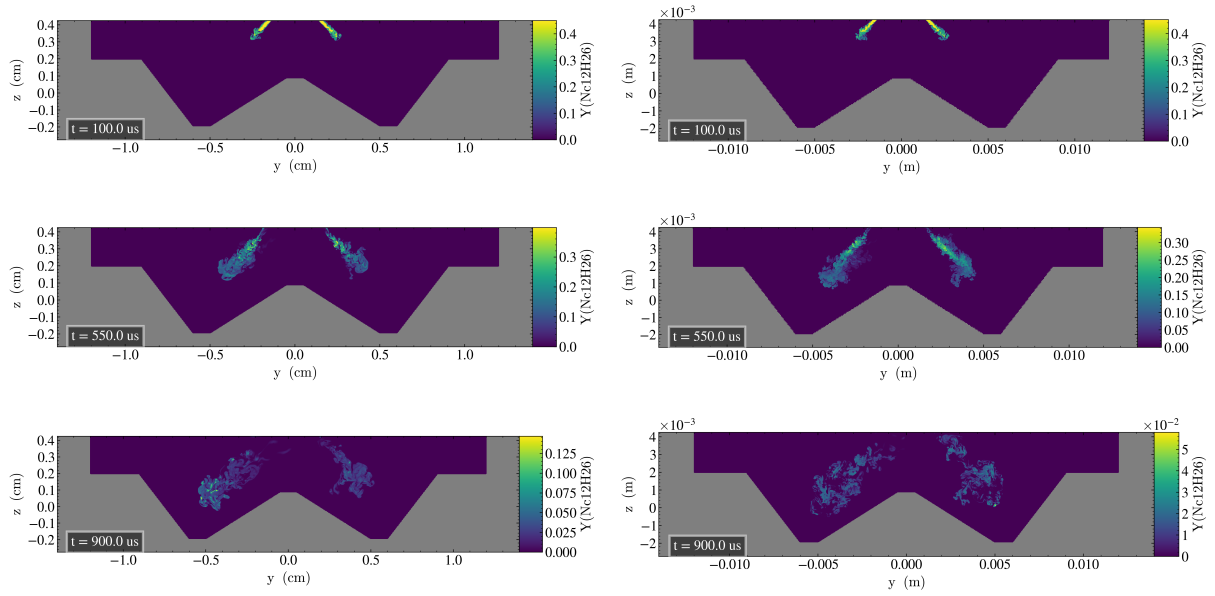

Figure 2: Development of fuel jets for three different snapshots of the RCCI simulation: 0.1 ms, 0.55 ms, 0.9 ms. PeleC results are in the first column and PeleLMeX results in the second.

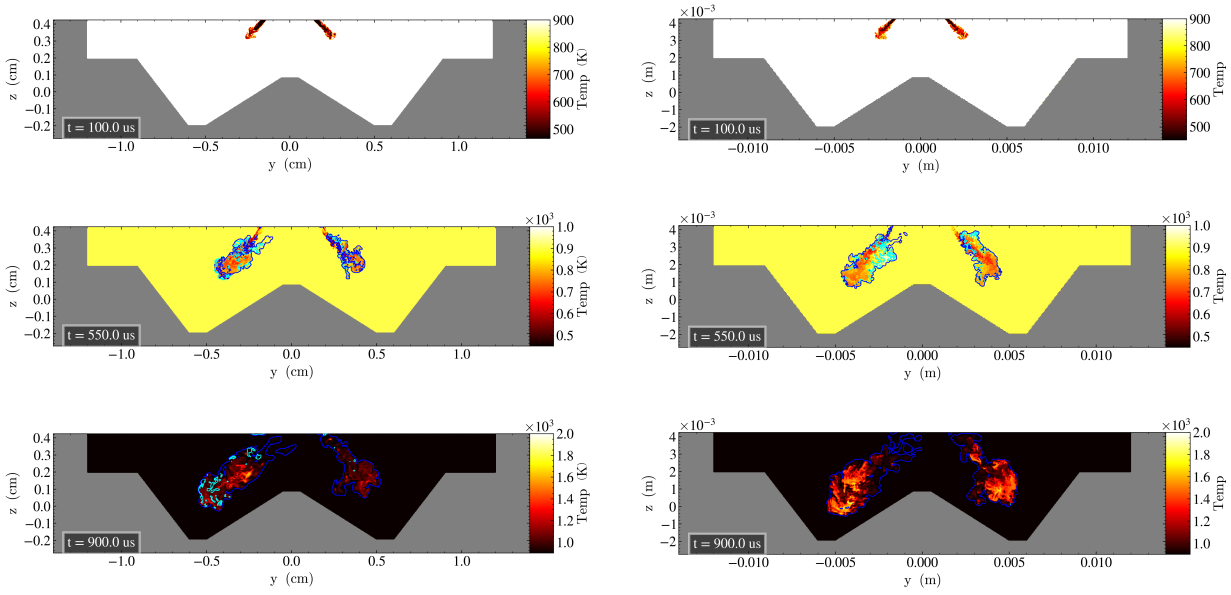

Figure 3: Temperature field and contours of species indicating low-temperature combustion for three different snapshots of the RCCI simulation: 0.1 ms, 0.55 ms, 0.9 ms. $Y(OC12H23OOH)$ at 1e-4 is shown in cyan and $Y(H2O2)$ at 1e-6 is shown in blue. PeleC results are in the first column and PeleLMeX results in the second.

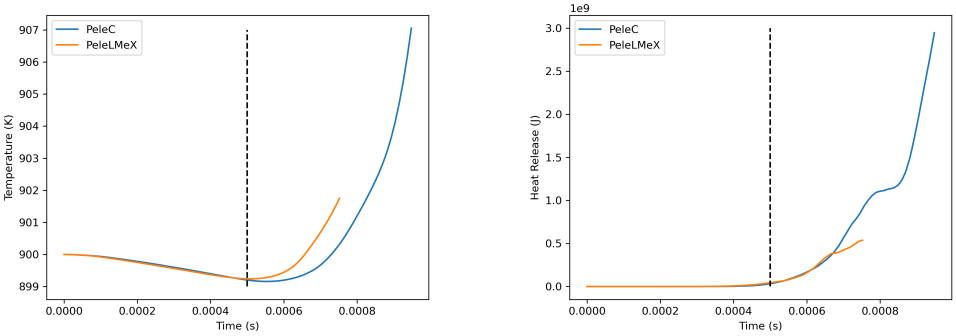

(a) Domain averaged temperature

(b) Domain averaged heat release

Figure 4: Domain averaged quantities weighted by cell volume as a function of time for both PeleC and PeleLMeX. The black dashed line indicates the end of the injection of fuel at 0.5 ms.

3.2 Quantitative comparisons

Figure 4 shows the domain averaged temperature and heat release for both PeleC and PeleLMeX as a function of time throughout the simulation. The averages where computed with a weighting factor based upon cell volume to account for the varying cell sizes inherent in an AMR based simulation. The black dashed line shows the point at which the fuel injection ends at 0.5 ms.

The average temperature lines (Figure 4(a) show close agreement early on in the simulation before 0.5 ms, but as the fuel injection stops, a recirculation region develops in the wake of the fuel streams and turbulent mixing dominates the flow field prior to ignition. It is at this part of the simulation where we see the main differences between the two solutions where the low-Mach number begins to auto-ignite sooner than the compressible solution.

Figure 4(b) shows the average heat release between PeleC and PeleLMeX. Here we see that the average heat release is in relatively good agreement up until about 0.7 ms, past the point at which the temperature averages start to deviate from one another. In both simulations there is a steady rise in the heat release as the first ignition kernels form until a point is reached at which the heat release plateaus; following a small dwell time, the heat release rises again rapidly signaling the onset of full ignition as the small ignition kernels spread and begin to consume the background methane/air mixture.

Figure 5 shows the average and standard deviation bands of the temperature conditioned on mixture fraction for the first half of the simulations at time instances from 0.1 ms to 0.5 ms. For the earlier time instances of the simulation, both PeleC and PeleLMeX show similar agreement in the mean, however the fully-compressible solution shows a significantly larger degree of variance, while the low-Mach solution has very small variance especially at the higher mixture fraction range. This initial variance in the fully-compressible solution is distributed uniformly across mixture fraction space and corresponds to compressive heating due to the pressure fluctuations within the cylinder. PeleLMeX does not display these variations across mixture fraction space since all pressure waves are removed from the simulation with the low-Mach formulation.

At 0.5 ms, we again see the beginning of the deviation between the solutions with the low-Mach solution starting to display an increase in the temperature at a mixture fraction of 0.05. PeleC also is beginning to develop an increase in this region, which can be seen in the standard deviation

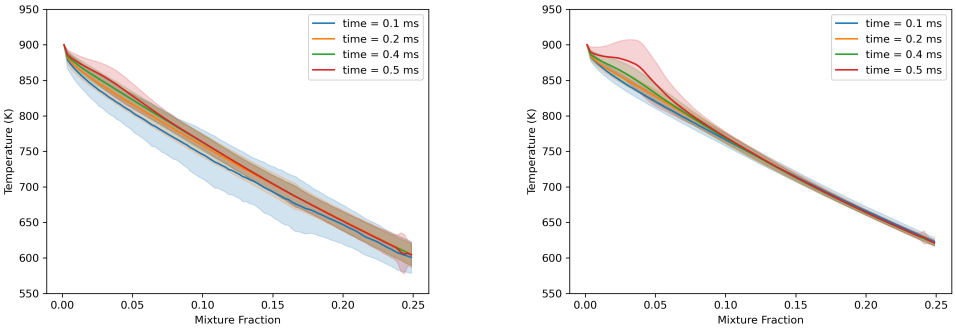

(a) PeleC (b) PeleLMeX

Figure 5: Conditional mean of temperature with standard deviation bands as a function of mixture fraction from 0.1 ms to 0.5 ms.

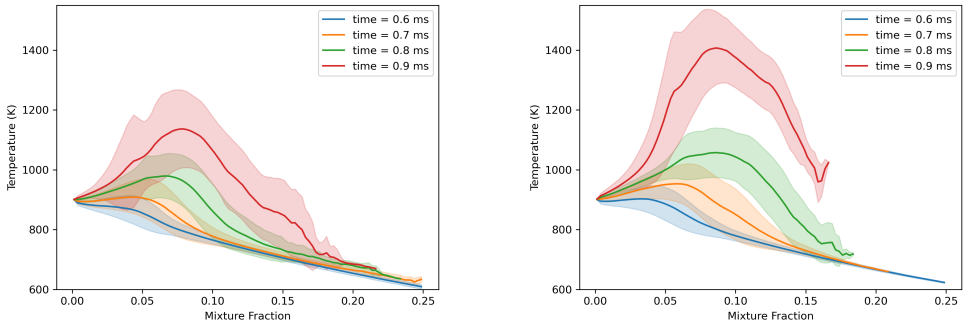

(a) PeleC (b) PeleLMeX

Figure 6: Conditional mean of temperature with standard deviation bands as a function of mixture fraction from 0.6 ms to 0.9 ms.

band, however, the mean has not been affected as much as in the low-Mach solution.

Figure 6 again shows the average of the temperature conditioned on mixture fraction, but for the second half of the simulation from time instances ranging from 0.6 ms to 0.9 ms. Here, all temperature profiles are displaying significant increases in temperature, initially at lower mixture fractions, but spreading to higher mixture fractions as the simulation progresses and the flame fills more of the domain. Based on the temperature profiles the compressible solution at 0.9 ms is more closely in agreement with the low-Mach solution at 0.8 ms, indicating a longer ignition delay in PeleC than in PeleLMeX.

Figure 7 shows the average scalar dissipation rate conditioned off of mixture fraction for both PeleC and PeleLMeX. The data show that for both simulations, the scalar dissipation rate is the highest at the beginning of the simulation when the fuel first penetrates into the ambient oxidizer and begins to mix together. As the simulations progress, the structure of the scalar dissipation rate changes. At the start of the simulations, the peak in scalar dissipation rate is near 0.055-0.075 mixture fraction, but the peaks shift initially downwards to a lower mixture fraction of 0.05, then to a higher mixture fraction of about 0.25 just before the onset of ignition, and finally the scalar

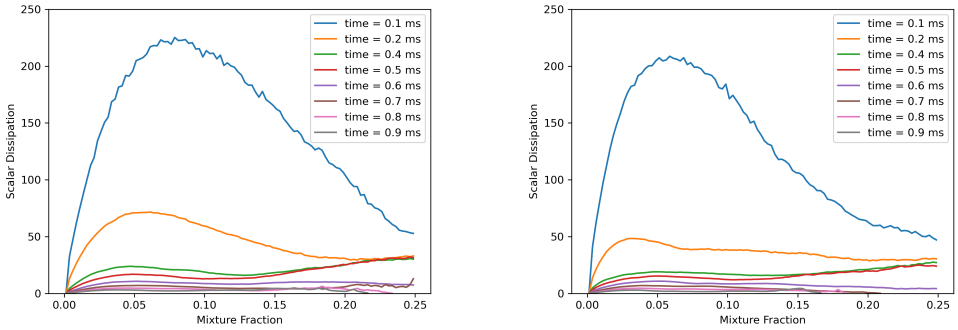

(a) PeleC (b) PeleLMeX

Figure 7: Conditional mean of scalar dissipation as a function of mixture fraction from 0.1 ms to 0.9 ms.

dissipation flattens out and becomes more equal across the full range of mixture fraction after the onset of the ignition event. For the full range of the simulation, the scalar dissipation rates are consistently higher in the PeleC simulation as compared to the PeleLMeX simulation, which acts to delay the onset of auto-ignition and is consistent with prior observations.

4. Conclusions

In this study, we have presented two exascale-ready CFD packages, one featuring a fully-compressible solver and the other a low-Mach approximation. Using both, we performed parallel high-resolution numerical simulations without a sub-grid scale model that approach the resolution required to be considered a DNS. We have shown that both solutions are capable of resolving the complex, real-world geometries associated with an RCCI engine using EBs and AMR. By examining the flow field and conditional statistics with respect to mixture fraction, we see that the onset of LTC in the simulation of the RCCI engine is sensitive to the mixing characteristics between the HRF injection and the surrounding LRF/air mixture. We have shown that the low-Mach solution auto-ignites faster than the fully-compressible solution resulting from the enhanced turbulent mixing and lower scalar dissipation rate than in the fully-compressible formulation. These results could have significant implications for future numerical studies of CI engines depending on the formulation used.

Acknowledgements

This research was supported by the Exascale Computing Project (ECP), Project Number: 17-SC-20-SC, a collaborative effort of two DOE organizations, the Office of Science and the National Nuclear Security Administration, responsible for the planning and preparation of a capable exascale ecosystem, including software, applications, hardware, advanced system engineering, and early testbed platforms to support the nation's exascale computing imperative.

References

[1] M. Badami et al., Experimental Investigation on Soot and NOx Formation in a DI Common Rail Diesel Engine with Pilot Injection, SAE Transactions 110 (2001) 663–674, URL: http://www.jstor.org/stable/44724341 (visited on 01/18/2023).

[2] D. Splitter et al., High Efficiency, Low Emissions RCCI Combustion by Use of a Fuel Additive, SAE International Journal of Fuels and Lubricants 3 (2010) 742–756, URL: http://www.jstor.org/stable/26272972 (visited on 01/18/2023).

[3] R. D. Reitz and G. Duraisamy, Review of high efficiency and clean reactivity controlled compression ignition (RCCI) combustion in internal combustion engines, Progress in Energy and Combustion Science 46 (2015) 12–71. DOI: https://doi.org/10.1016/j.pecs.2014.05.003.

[4] A. Bhagatwala et al., Numerical investigation of spontaneous flame propagation under RCCI conditions, Combustion and Flame 162 (2015) 3412–3426.

[5] M. B. Luong et al., Ignition of a lean PRF/air mixture under RCCI/SCCI conditions: A comparative DNS study, Proceedings of the Combustion Institute 36 (2017) 3623–3631.

[6] G. H. Yu et al., Ignition characteristics of a temporally evolving n-heptane jet in an iso-octane/air stream under RCCI combustion-relevant conditions, Combustion and Flame 208 (2019) 299–312.

[7] B. Tekgül et al., Large-eddy simulation of split injection strategies in RCCI conditions, Combustion Theory and Modelling (2022) 1–22.

[8] M. Day et al., Pele: an exascale-ready suite of combustion codes, tech. rep. Report No. PR-2C00-82880, National Renewable Energy Lab. (NREL), 2022.

[9] M. T. Henry de Frahan et al., PeleC: An adaptive mesh refinement solver for compressible reacting flows, The International Journal of High Performance Computing Applications (2022) 10943420221121151.

[10] M. Day et al., PeleLMeX, tech. rep. Report No. NREL SWR-22-48, National Renewable Energy Lab. (NREL), Lawrence Berkeley National Lab. (LBNL), 2022.

[11] W. Zhang et al., AMReX: a framework for block-structured adaptive mesh refinement, Journal of Open Source Software 4 (2019) 1370–1370.

[12] P. Team, PelePhysics, a repository of physics databases and implementation code for use with the Pele suite, 2022, URL: https://github.com/AMReX-Combustion/PelePhysics.

[13] C. J. Balos et al., Enabling GPU accelerated computing in the SUNDIALS time integration library, Parallel Computing 108 (2021) 102836.

[14] A. Nonaka et al., A conservative, thermodynamically consistent numerical approach for low Mach number combustion. Part I: Single-level integration, Combustion Theory and Modelling 22 (2018) 156–184.

[15] A. Abdelfattah et al., Fast Cholesky factorization on GPUs for batch and native modes in MAGMA, Journal of Computational Science 20 (2017) 85–93.